PROPOSED HIGHER ORDER CONTINUUM-BASED MODELS FOR AN ELASTIC SUBGRADE

Asrat Worku
Department of Civil Engineering
Addis Ababa University

ABSTRACT

Three new variants of continuum-based models for an elastic subgrade are proposed. The subgrade is idealized as a homogenous, isotropic elastic layer of thickness H overlying a firm stratum. All components of the stress tensor in the subgrade are taken into account. Reasonable assumptions are made regarding the depth-wise variation of the vertical shear stress components and of the horizontal-to-vertical normal stress ratios to simplify mathematical work. The assumptions are based on observation of available analytical results of stress distributions and on knowledge of lateral earth pressure theories. The resulting differential equations are similar in form and order to a high-order model developed earlier by Reissner based on a number of simplifying assumptions, but with different coefficients dependant on Poisson ratio. With the help of appropriately selected mechanical models, it has been shown that all of the new model variants consistently give larger effective vertical stiffness and larger shear interaction among the classical Winkler springs for the range of Poisson ratio of practical interest.

Keywords: *Continuum models, Kerr model, Mechanical models, Reissner model, Shear interaction, Winkler model.*

INTRODUCTION

Subgrade models developed so far can be categorized into two classes: continuum-based and mechanical models. A number of mechanical models have been proposed in the past having varying degrees of mathematical complexity and different numbers of model parameters [1-6]. These models range from the classical single-parameter Winkler model to the multi-parameter models of Rhines [3,4]. In contrast, continuum-based subgrade models proposed in the past are relatively few in number. Reissner's simplified continuum model (RSCM) can be regarded as one of the pioneering works based on some direct simplifying assumptions [3,4,7,8]. Horvath used later on two modifications of Reissner model to study the behavior of mat foundations [3,7]. Vlasov and Leont'ev presented a relatively indirect application of the simplified continuum that involves variational calculus [9].

The RSCM makes the simplifying assumption of zero in-plane stresses; i.e. $\sigma_x = \sigma_y = \tau_{xy} = 0$ [8]. The works of Horvath are also based on the same assumption [3,7]. The consequence of this assumption is that the vertical shear stress components become constant and the vertical normal stress component varies linearly with depth. This assumption considerably simplifies the mathematical work needed in arriving at the mathematical model, which is a second-order differential equation with constant coefficients. However, it underestimates both the vertical stiffness of the subgrade and the inherent shear interaction rendering the model one of the most conservative.

The present work follows Reissner's approach, but without neglecting any stress components. Instead, three different combinations of assumptions are made with regard to the lateral normal and the vertical shear stress components resulting in three correspondingly different variants of subgrade models.

In the first model variant, a linear relationship between the horizontal and the vertical normal stress components is assumed. This assumption has as its basis the classical theory of lateral earth pressure, in which linear relationships are assumed between the normal stresses, whether one deals with active, passive or at-rest lateral earth pressure condition. The other assumption in this model is a constant depth-wise variation of the vertical shear stress components.

In the second model variant, whereas the first assumption in the first variant with respect to the horizontal normal stresses is maintained, the second assumption with respect to the vertical shear stresses is improved by assuming a bilinear depth-wise variation. This second assumption is introduced as a reasonable approximation of the nonlinear variation of the shear stresses observed in plots of analytical results available in the literature [10].

The third model variant is derived by maintaining the second assumption in the second variant with respect to the vertical shear stresses and introducing an exponentially decaying function to approximate the vertical variation of the ratio of the horizontal to the vertical normal stresses. Once again, plots of available analytical results of the normal stresses are used to support this assumption [10].

Interestingly, all of the three model variants result in differential equations similar in form and order to that of RSCM, but exhibiting notable differences in their coefficients. A synthesis of these models with equivalent mechanical models helps in interpreting the differences observed in the coefficients of the differential equations. For this purpose, the Kerr mechanical model is used. Comparisons show that all of the new model variants brought about increases in the vertical stiffness of the subgrade and the shear interaction among the Winkler springs.

There is a trend of increasing interest in numerical and analytical studies of beams and plates on elastic foundations using such models [11-15]. Similar studies on beams and plates using various subgrade models that include the variants reported in this work are currently underway with the objective of corroborating the findings presented here based on theoretical considerations alone. Numerical results found so far are encouraging. It appears possible to calibrate these models so that they give results in excellent agreement with finite-element based models.

THE PROPOSED MODELS

In all model variants proposed in this work, the subgrade under consideration is similar to that of RSCM, which consists of a homogenous, isotropic elastic layer of thickness *H* underlain by a rigid formation as shown in Fig 1. The layer is characterized by its elastic parameters of Young's modulus, *E*, and Poisson's ratio, ν [8]. At the depth *H*, all deformation components are assumed zero.

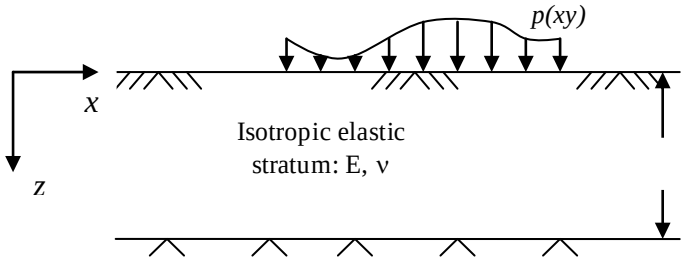

Figure 1 The elastic soil layer of thickness *H* overlying a rigid stratum

The difference between the stress tensors of the RSCM and the present model variants is as shown in the arrays below in accordance with the Cartesian coordinate system:

RSCM

$$\begin{pmatrix} 0 & 0 & \tau_{xz} \\ 0 & 0 & \tau_{yz} \\ \tau_{xz} & \tau_{yz} & \sigma_z \end{pmatrix}$$

NewVariants

$$\begin{pmatrix} \sigma_x & \tau_{xy} & \tau_{xz} \\ \tau_{xy} & \sigma_y & \tau_{yz} \\ \tau_{xz} & \tau_{yz} & \sigma_z \end{pmatrix}$$

In the RSCM, the three independent in-plane stress components are neglected (i.e. $\sigma_x = \sigma_y = \tau_{xy} = 0$). As a consequence, the two remaining shear stress components, τ_{xz} and τ_{yz}, become constant with respect to depth, and the only non-zero normal stress component, σ_z, varies linearly with depth. In contrast, no stress component is neglected in any of the models proposed in this work as shown in the array on the right-hand side. The proposed three models differ from each other according to the assumptions made with regard to the depth-wise variation of the vertical shear stress components, τ_{xz} and τ_{yz}, and the ratio of the lateral normal stress components, σ_x and σ_y, to the vertical normal stress, σ_z. Simplifying assumptions with regard to the rest of the stress components are unnecessary.

Model variant 1

This model, referred to simply as Variant 1, is based on the following two basic assumptions:

i. The horizontal normal stresses, σ_x and σ_y, are linearly related to the vertical normal stress, σ_z; i.e. $\sigma_x = k_x \sigma_z$ and $\sigma_y = k_y \sigma_z$. Knowledge of lateral earth pressure theories motivated this assumption and can be utilized to reasonably estimate the values of the coefficients k_x and k_y. Specifying values for the coefficients in advance is not necessary for the derivation of the model.

ii. The vertical shear stress components, τ_{xz} and τ_{yz}, are assumed constant with depth. This assumption is made only for the sake of mathematical ease and in order to show that RSCM is a simplified form of this model variant. This assumption results in a linear depth-wise variation of the vertical normal stress, σ_z.

Pertinent stress equations, strain-displacement relations, Hooke's law for isotropic elastic materials, and the boundary conditions at the ground surface and at the interface with the rigid formation are utilized to derive the mathematical model, the details of which are presented in Appendix A.

The resulting subgrade model relating the surface pressure $p(x, y)$ and the corresponding surface displacement $w_0(x, y)$ is given by

$$p(x,y)-\alpha\left(\frac{GH^2}{12E}\right)\nabla^2 p(x,y)=\frac{1}{\alpha}\frac{E}{H}w_0(x,y) -\frac{GH}{3}\nabla^2 w_0(x,y) \quad (1a)$$

In this second order partial differential equation with constant coefficients, G is the shear modulus of the upper layer, and the coefficient α is given by the relation

$$\alpha=1-\nu\left(k_x+k_y\right) \quad (2)$$

For $k_x = k_y = 0$ (or zero lateral normal stresses), the coefficient α becomes unity, and Eq. (1a) reduces to the form of RSCM [8] given by

$$p(x,y)-\frac{GH^2}{12E}\nabla^2 p(x,y)=\frac{E}{H}w_0(x,y) -\frac{GH}{3}\nabla^2 w_0(x,y) \quad (1b)$$

If the higher derivatives in Eqs. (1a) and (1b) are dropped, Winkler-type models are obviously recovered. If the coefficients k_x and k_y are assumed to be equal to the lateral earth pressure coefficient for at rest condition, k_0, and noting that this coefficient can be expressed as $k_0=\nu/(1-\nu)$, then α in Eq. (1a) takes the form

$$\alpha=\frac{1-\nu-2\nu^2}{1-\nu} \quad (3)$$

According to this relation, α is always less than one tending to zero with ν approaching 0.5. For ν=0.5, Eq. (3) becomes indeterminate. However, the coefficients k_x and k_y can generally be selected different from k_0, and k_0 can also be expressed in terms of other soil properties like the strength parameters or the degree of consolidation.

Model variant 2

This model, referred to as Variant 2, is based on the following assumptions:

i. The horizontal normal stresses, σx and σy, are linearly related to the vertical normal stress, σ_z, as in Variant 1.

ii. The vertical shear stress components, τ_{xz} and τ_{yz}, are assumed to vary with depth according to a bilinear relation. This assumption emanates from observation of plots of the stress components underneath a uniformly loaded circular region on the surface of an elastic half space. These plots are prepared from tabular values provided by Das [10] citing the works of Ahlvin and Ullery and are given in Fig. 2(a) for different vertical planes.

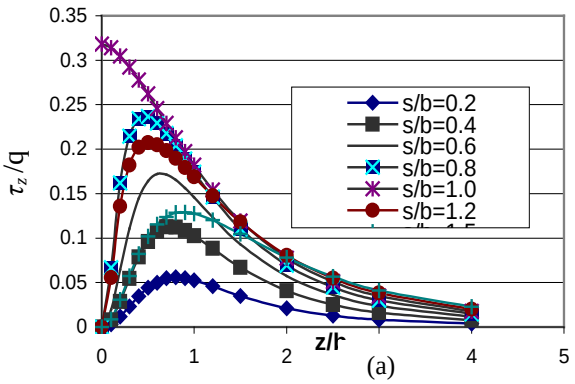

(a)

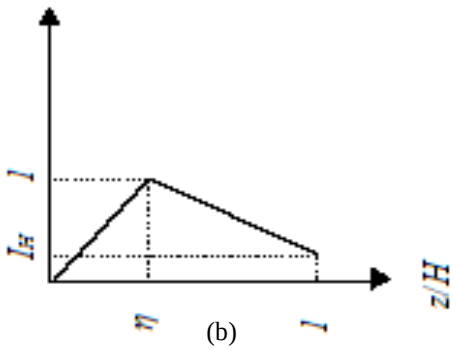

(b)

Figure 2 (a) Plots of the vertical shear stress with depth for a circular region subjected to a uniformly distributed load; (b) A qualitative plot of the influence factor $I(z)$

In Fig. 2(a), *b* is the radius of the loaded circular region and *s* is the radial coordinate in accordance with the cylindrical coordinate system, the origin of which is taken as the center of the circle. All the curves in Fig. 2(a) exhibit a similar trend, and their peaks occur within a narrow band of *z*. An exception is the curve for points below the edge of the circle due to the discontinuity there. Plots of shear stresses exhibiting a similar trend are also reported by Horvath for points beneath a loaded square region on the surface of a layered formation [7].

The plots in both Fig. 2(a) and in Horvath [7] suggest the use of the following bilinear variation for the vertical shear stress components with depth:

$$\tau_{xz}(x,y,z) = I(z)\bar{\tau}_{xz}(x,y) = \begin{cases} (b_1 z)\,\bar{\tau}_{xz}(x,y); & \text{if } 0 \le z \le \eta H \\ (a_2 + b_2 z)\bar{\tau}_{xz}(x,y); & \text{if } \eta H \le z \le H \end{cases} \quad (4)$$

where $\bar{\tau}_{xz}(x,y)$ gives the variation of τ_{xz} in the horizontal *x*, *y*-plane, and *I*(*z*) is the depth-dependant influence factor assumed to vary bi-linearly. A qualitative plot of *I*(*z*) is given in Fig. 2(b). This assumption results in a quadratic variation of the vertical stress, σ_z, unlike the linear variation in Variant 1 and RSCM. The coefficients a_2, b_1, and b_2 characterizing the two line segments of *I*(*z*) can be readily determined from the known coordinates of the three points in Fig. 2(b) - the origin, the peak and the lower-most point.

As in Variant 1, all pertinent elasticity equations together with the boundary conditions are employed to derive the mathematical model, the details of which are given in Appendix B. In addition, continuity of deformation at the depth $z = \eta H$ is taken into consideration. The corresponding mathematical model of the subgrade becomes

$$p(x,y) - \frac{\alpha\beta G\xi_p}{HE}\nabla^2 p(x,y) = \frac{E}{\alpha H} w_0(x,y) - \frac{\beta G\xi_w}{H}\nabla^2 w_0(x,y) \quad (5a)$$

Where $\xi_p = \xi_1/\xi_3$ and $\xi_w = \xi_2/\xi_3$. The coefficients β, ξ_1, ξ_2, and ξ_3 in Eq. (5a) are provided in Appendix B. The coefficient α is as defined in Eqs. (2) for the first new variant.

For thick elastic strata, the depth-wise variation of the vertical shear stresses shown in Fig. 2 for an elastic half space may be taken as sufficiently representative for most foundations. The thickness *H* may be taken as that, beyond which the shear stress becomes negligibly small. The corresponding value of I_H at this depth may be taken around 0.1. Furthermore, the normalized average depth, at which the shear stresses assume peak values, may be taken as $\eta = 0.6$ in both cases.

With the peak and the lower-most points in Fig. 2(b) so established, the influence curve for the vertical shear stresses is fully defined and the various constants in the coefficients of Eq. (5a) can be readily evaluated from the relations given in Appendix B. Substituting these coefficients, one obtains the following relation for the subgrade model sought:

$$p(x,y) - 2.35\alpha\left(\frac{GH^2}{12E}\right)\nabla^2 p(x,y) = \frac{1}{\alpha}\frac{E}{H} w_0(x,y) - 2.22\left(\frac{GH}{3}\right)\nabla^2 w_0(x,y) \quad (5b)$$

Comparison of Eq. (5b) with (1a) and (1b) shows that the three models are still similar in form, but exhibit differences in their coefficients.

If the higher derivatives in Eq. (5b) are dropped, one obtains the same Winkler-type model as in Variant 1, because the two models differ from each other only in the depth-wise variation of the vertical shear stresses - a condition irrelevant in Winkler model, which entirely ignores the shear stresses.

If the coefficients k_x and k_y are assumed equal to the lateral earth pressure coefficient for at rest condition, k_0, as in the previous model, then α can be determined from Eq. (2) for any value of ν.

Model variant 3

In this variant, whereas the second assumption in Variant 2 of bilinear variation of the vertical shear stress components with depth is maintained, the first assumption of a linear relation between the normal stress components is replaced by the decaying exponential functions of the form:

$$\sigma_x = r_x e^{-\zeta z}\sigma_z; \quad \sigma_y = r_y e^{-\zeta z}\sigma_z \quad (6)$$

where r_x, r_y, and ς are constants. This assumption is motivated by observation of plots of σ_r/σ_z for points directly below a circular region of diameter equal to the layer thickness on the surface of an elastic half space subjected to a uniformly distributed vertical load, where σ_r is the radial normal stress and σ_z is the vertical normal

stress [10]. An exponential function of the type of Eq. (6) tallies excellently with the plots, from which the constants r_x, r_y, and ς can be easily estimated.

Horvath gave plots of the normal stresses for points below a vertically loaded square region of side length *B* on a layered half space [3]. These plots also suggest the use of relations similar to Eq. (6) for depths of up to around *0.7B*, especially for points directly below the loaded region.

All pertinent elasticity equations together with the boundary and continuity conditions are employed to derive the mathematical model, the details of which are described in Appendix C. The resulting mathematical model takes the form

$$p(x,y)-\frac{\lambda G\kappa_p}{\delta E}\nabla^2 p(x,y)=\frac{E}{\delta}w_0(x,y) -\frac{\lambda G\kappa_w}{\delta}\nabla^2 w_0(x,y) \qquad (7a)$$

Where $\kappa_p=\kappa_1/\kappa_3$ and $\kappa_p=\kappa_2/\kappa_3$. Expressions for the coefficients λ, δ, κ_1, κ_2, and κ_3 in Eq. (7a) are given in Appendix C. Observation of the plots suggests the use of the following function:

$$\sigma_x=\sigma_y=0.8e^{-3.96z/H}\sigma_z$$

The same bilinear depth-wise variation of the vertical shear stresses shown in Fig. 2 is taken with I_H =0.1 and η=0.6. Once the depth-wise variations of the lateral normal stresses and of the vertical shear stresses are known, the coefficients in Eq. (7a) can be readily evaluated in terms of the Poisson's ratio and the layer thickness *H* using the relations provided in Appendix C. Accordingly, one obtains

$$\begin{aligned}
\delta &= (1-0.404\nu)H \\
\lambda &= (0.236+1.286\nu)H^2 \\
\kappa_p &= \left(\frac{1}{23.68}\frac{\nu\delta}{\lambda}H-\frac{1}{17.72}\frac{\delta}{\lambda}H+\frac{1}{22.46}\frac{\nu}{\lambda}H^2-\frac{1}{3.71}\nu+0.19\right)H \\
\kappa_w &= 1.15+\frac{H^2}{17.72\lambda}+\frac{H^2}{66.8}\frac{\nu}{\lambda}
\end{aligned} \qquad (7b)$$

The coefficients in the brackets and in the expression for κ_w are dimensionless quantities and dependent only on the Poisson ratio that can be easily evaluated. Once again, the differences in the coefficients of this and the previous mathematical models are to be noted on the coefficients.

One can note from the forgoing material that all the proposed continuum-based models have the same form and order as the RSCM. All involve the functions *p* and w_0 and their respective second derivatives. The trend suggests that the likelihood of the occurrence of other terms and other orders of derivatives is unlikely with further refinement of assumptions. A recently published work of the author that generalizes the presented approach of subgrade modeling showed that the maximum order of the differential equation and its general form remain indeed unchanged [15].

SYNTHESIS OF THE PROPOSED CONTINUUM-BASED MODELS WITH A PERTINENT MECHANICAL MODEL

The synthesis of continuum-models with pertinent mechanical models provides a means of quantifying the mechanical model parameters from those of the continuum. It also provides a useful perspective to compare the continuum models with each other. Looking at the form and order of the governing differential equations of the subgrade models presented above, the most appropriate mechanical model for this purpose is the three-parameter Kerr model [4].

This model consists of two beds of springs with spring constants of k_u and k_l per unit area separated by a shear layer of parameter g_k as shown in Fig. 3.

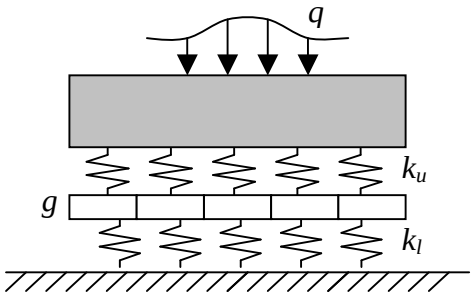

Figure 3 The Kerr (or modified-Pasternak) mechanical model

The governing differential equation of this model as derived by Kerr is given by [4]

$$p(x,y)-\frac{g_k}{(k_u+k_l)}\nabla^2 p(x,y)=\frac{k_l k_u}{(k_u+k_l)}w_0(x,y) -\frac{g_k k_u}{(k_u+k_l)}\nabla^2 w_0(x,y) \qquad (8)$$

Equation (8) is similar in form and order to the equations of all continuum-based models presented

above. Equating the coefficients in Eq. (8) with the corresponding coefficients in Eqs. (1a), (1b), (5b) and (7a) provides in each case three equations. Simultaneous solution of these equations yields different expressions for the mechanical model parameters, which are summarized below together with the effective stiffness coefficient established using the relation $k_e = k_u k_l / (k_u + k_l)$ for the springs in Fig. 3 that are arranged in series:

Kerr Parameters from RSCM

$$k_u = \frac{4E}{H}; \quad k_l = \frac{4E}{3H}; \quad g = \frac{4GH}{9}; \quad k_e = \frac{E}{H} \tag{9}$$

Kerr Parameters from Variant 1

$$k_u = \frac{4E}{\alpha H}; \quad k_l = \frac{4E}{\alpha 3H}; \quad g = \frac{4GH}{9}; \quad k_e = \frac{E}{\alpha H} \tag{10}$$

Kerr Parameters from Variant 2

$$k_u = \frac{\xi_w}{\xi_p}\frac{E}{\alpha}; \quad k_l = \frac{\xi_w}{\left(H\xi_w - \xi_p\right)}\frac{E}{\alpha};$$
$$g = \frac{\xi_w^2}{\left(H\xi_w - \xi_p\right)}\beta G; \quad k_e = \frac{E}{\alpha H} \tag{11}$$

Kerr Parameters from Variant 3

$$k_u = \frac{\kappa_w}{\kappa_p}E; \qquad k_l = \frac{\kappa_w}{\left(\delta\kappa_w - \kappa_p\right)}E;$$
$$g = \frac{\kappa_w^2}{\left(\delta\kappa_w - \kappa_p\right)}\lambda G; \qquad k_e = \frac{1}{1 - 0.404\nu}\frac{E}{H} \tag{12}$$

Comparison of the relations in Eqs. (9) and (10) shows that the spring constants of Variant 1 are always $1/\alpha$ times those of RSCM. Since the factor α is always less than unity for common values of Poisson ratio of soils, both the individual bed of springs and the effective spring of Variant 1 are always stiffer than that of RSCM. In contrast, the shear parameter remained unchanged as could be expected, because constant vertical shear stresses are either assumed or implied in both models.

The parameters from Variant 2 become clearer by introducing the pertinent relations for the bilinear variation of the vertical shear stress components. This yields $\xi_p = -0.35H$ and $\xi_w = -1.31$, which when inserted in Eqs. (11) give

$$k_u = 3.75\frac{E}{\alpha H}; \quad k_l = 1.36\frac{E}{\alpha H}; \quad g = GH \tag{13}$$

These relations show that even though the effective spring coefficient remains the same in both Variant 1 and Variant 2, the individual spring beds are different. The shear parameter of Variant 2, on the other hand, has increased significantly to 2.25-fold that of RSCM and Variant 1 irrespective of the Poisson ratio. Therefore, Variant 2 predicts significantly higher stiffness and higher shear interaction of the subgrade as compared to RSCM, especially for soils with larger Poisson ratio.

With the introduction of the bilinear variation for the vertical shear stresses and the decaying exponential function for the ratio of the lateral to vertical normal stresses, the various constants in Eqs. (12) can be determined from Eqs. (7b). Then, the coefficients of the individual spring beds and the shear parameter can be easily evaluated. For two selected values of Poisson ratio, this gives:

For $\nu = 0.3$:

$$k_u = 17.7\frac{E}{H}; \quad k_l = 1.22\frac{E}{H}; \quad k_e = 1.14\frac{E}{H}; \quad g = 0.95GH$$

For $\nu = 0.45$:

$$k_u = 21.3\frac{E}{H}; \quad k_l = 1.30\frac{E}{H}; \quad k_e = 1.22\frac{E}{H} \quad g = 1.30GH$$

These expressions show that Variant 3 predicts always a shear parameter much higher than Variant 1 and RSCM, and even larger than Variant 2 for Poisson ratio larger than about 0.33.

Plots of Kerr Parameters

The three normalized Kerr parameters are plotted in Fig. 4 against Poisson ratio.

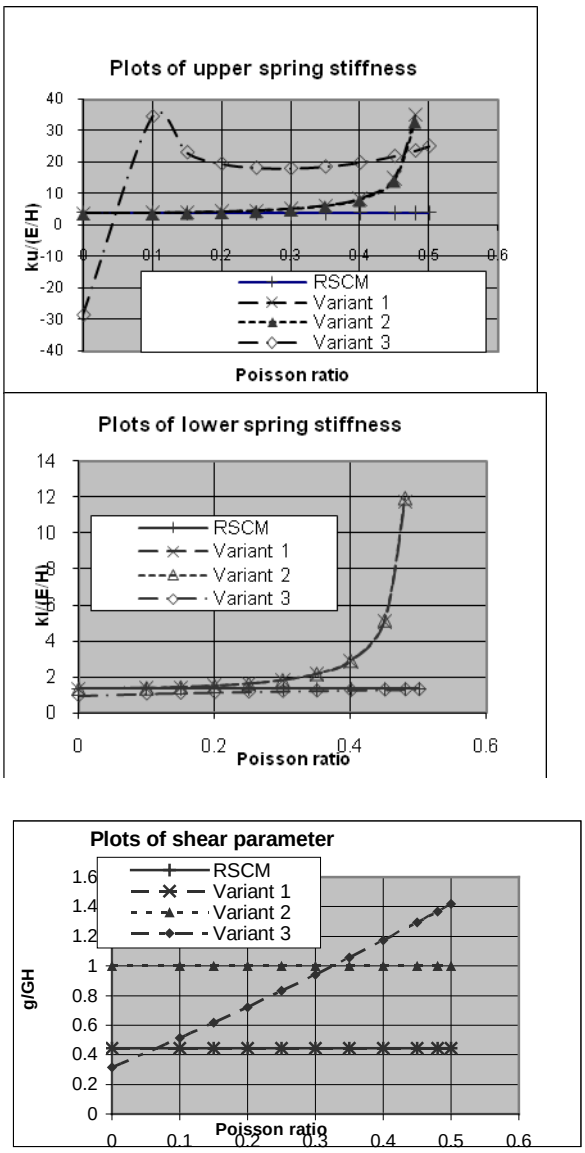

Figure 4: Plots of the normalized model parameters against Poisson ratio as predicted by different continuum-based models

The following important observations can be made from these normalized plots within the common range of values of Poisson ratio:

1. The three parameters of the RSCM are all independent of Poisson ratio and always less than those of the new model variants. This model is thus the most conservative of all.

2. The increase in the normalized spring stiffness values from 1.0 at ν =0 to 1.25 at ν=0.5 in Variant 3 is slow as compared to the rate of increase observed in Variants 1 and 2. Furthermore, the stiffness does not become indeterminate at $\nu = 0.5$. This is due to the more realistic decaying exponential function used in Variant 3 for the normal stress ratios in lieu of a constant.

3. In the important range of Poisson ratio of soils, Variant 3 represents the highest shear parameter of all that increases nearly linearly with increasing values of ν. This variation can be approximated by $g_k /(GH) = 2.317\nu + 0.259$. The shear parameter of Variant 3 for $\nu = 0.5$ is more than threefold that of RSCM and Variant 1 and about 40% larger than that of Variant 2.

CONCLUSIONS

From the foregoing material, the following conclusions are drawn:

1. The RSCM consistently underestimates both the vertical stiffness and the inherent shear interaction of the subgrade.

2. The highest shear interaction is achieved in Variant 3, especially for large Poisson ratios, by combining the assumption of bilinear vertical shears with the assumption of an exponentially decaying vertical-to-horizontal normal stress ratio with depth. However, the increase in the vertical stiffness is not as large as in the other two model variants.

3. Considering the reasonable assumptions they are based on, Variant 2 and Variant 3 are promising alternatives to existing continuum subgrade models.

4. Results of recently completed studies on beams using these models indicate that the new models, in particular Variant 3, can be easily calibrated to give results in excellent agreement with finite-element based models.

REFERENCES

[1] Fletcher, D. Q. and Hermann L. R. Elastic Foundation Representation of Continuum. *Journal of Engineering Mechanics*, ASCE, 1971, 97, No. EM1, 95-107

[2] Hetényi, M. *Beams on Elastic Foundation*, University of Michigan Press, Ann Arbor, 1946.

[3] Horvath, J. S. Basic SSI Concepts and Applications Overview. Soil-Structure

Interaction Research Project, Report No. CGT-2002-2, Manhattan College, New York, 2002.

[4] Kerr, A. D. Elastic and Viscoelastic Foundation Models. *Journal of Applied Mechanics*, ASME, 1964, 25 (80); 491-498.

[5] Selvadurai, A. P. S. *Elastic Analysis of Soil-Foundation Interaction*. Elsevier Scientific Publishing Company, New York, 1979.

[6] Wang, H., Tham, L. G., Cheung, Y. K. Beams and Plates on Elastic foundations: a review. *Progress in Structural Engineering and Materials*, John Wiley 2005, 7; 174-182.

[7] Horvath J. S. New Subgrade Model Applied to Mat Foundations. *Journal of Geotechnical Engineering*, ASCE, 1983, 109 (12); 1567-1587.

[8] Reissner, E. A Note on Deflections of Plates on a Viscoelastic Foundation. *Journal of Applied Mechanics*, ASME, 1958, 25 (80); 144-145.

[9] Vlasov, V. Z., Leont'ev, N. N. Beams, Plates, and Shells on Elastic Foundations. *Israel Program for Scientific Translations*, Jerusalem, 1966 (Translated from Russian, 1960).

[10] Das, B. M., *Advanced Soil Mechanics*, McGraw-Hill Book Company, New York, 1983.

[11] Avramidis, I. E., Morfidis, K. Bending of Beams on Three-Parameter Elastic Foundation. *International Journal of Solids and structures*, Elsevier, 2006, 43; 357-375.

[12] Nogami T., O'Neill, M. W. Beam on Generalized Two-Parameter Foundation. *Journal of Engineering Mechanics*, ASCE, 1985, 111, 5; 664-679.

[13] Tanahashi, H. Formulas for an Infinitely Long Bernoulli-Euler Beam on the Pasternak Model. *Soils and Foundations*, Japanese Geotechnical Society, 2004, 44, 5; 109-118.

[14] Tanahashi, H., Pasternak Model Formulation of Elastic Displacements in the Case of a Rigid Circular Foundation. *Journal of Asian Architecture and Building Engineering*, 2007, 6, 1; 167-173.

[15] Worku, A. "Part I: A generalized Formulation of Continuum Models for Elastic Foundations," accepted for presentation and publication, GeoFlorida 2010, Annual Conference of the Geo-Institute, American Society of Civil Engineers, February 20-24, 2010.

[16] Yin, J. H. Closed-Form Solution for Reinforced Timoshenko Beam on Elastic Foundation. (Technical Note) *Journal of Engineering Mechanics*, ASCE, 2000, 126, 8; 869-874.

APPENDICES

Appendix A: Derivation of Model 1

Equation (1a) is derived following the same procedure as in Reissner's and Horvath's work [2,3].

The stress equilibrium equation in the vertical direction is given by

$$\sigma_{z,z} + \tau_{zx,x} + \tau_{zy,y} = 0 \qquad \text{(A1)}$$

Assuming that the vertical shear stresses are constant with depth, integrating Eq. (A1) with respect to z, and employing the stress boundary condition at the surface, one obtains

$$\sigma_z = -Qz - p \qquad \text{(A2)}$$

Substituting Eq. (A2) in the combined stress-strain and strain-displacement equation for the vertical direction, noting the assumption $\sigma_x = k_x\sigma_z$, *and* $\sigma_y = k_y\sigma_z$, integrating with respect to z, and employing the displacement boundary conditions at the surface and at the bottom of the layer, one obtains the following relations:

$$w(x,y) = w_0 - \frac{\alpha}{E}\left[\frac{Qz^2}{2} + pz\right] \qquad \text{(A3)}$$

where

$$Q = \frac{2}{H^2}\left(\frac{E}{\alpha}w_0 - pH\right) \qquad \text{(A4)}$$

and

$$\alpha = 1 - \nu\left(k_x + k_y\right) \qquad \text{(A5)}$$

Equation (A3) is now substituted in the combined equations of stress-strain and strain-displacement for the vertical shear stresses given by

$$\begin{aligned} u_{,z} + w_{,x} &= \tau_{xz}/G \\ v_{,z} + w_{,y} &= \tau_{zy}/G \end{aligned} \qquad \text{(A6)}$$

Equations (A6) are integrated with respect to z and the remaining displacement boundary conditions applied. The resulting equations are solved for the shear stresses to yield

$$\begin{aligned} \tau_{xz} &= \frac{2G}{3}w_{0,x} - \frac{\alpha GH}{6E}p_{,x} \\ \tau_{yz} &= \frac{2G}{3}w_{0,y} - \frac{\alpha GH}{6E}p_{,y} \end{aligned} \qquad \text{(A7)}$$

Finally, Eqs. (A2) and (A7) are inserted in Eq. (A1) and rearranged to obtain

$$p(x,y) - \alpha\left(\frac{GH^2}{12E}\right)\nabla^2 p(x,y) = \frac{1}{\alpha}\frac{E}{H}w_0(x,y) - \frac{GH}{3}\nabla^2 w_0(x,y) \qquad \text{(A8)}$$

Equation (A8) is the differential equation for Variant 1 given in Eq. (1a).

Appendix B: Derivation of Model 2

Equation (5a) is derived in a similar manner as that of Eq. (A8) above, except that the continuity condition of displacements at $z = \eta H$ should be observed in addition to the boundary conditions. This involves a relatively lengthy mathematical work. For brevity reasons, only the final forms of the coefficients are given below:

$$\beta = (3-2\eta)\frac{(b_1-b_2)}{6}\eta^2H^3 + \frac{b_2}{6}H^3 + (1-2\eta)\frac{a_2H^2}{2} \qquad \text{(A9)}$$

$$\xi_1 = -\frac{b_1}{24\beta}H(\eta H)^4 + \left(\eta - \frac{1}{2}\right)H^2 + \frac{H}{\beta}\left(\overline{P}_{\eta H} - \overline{P}_H\right) \qquad \text{(A10)}$$

$$\xi_2 = -\frac{b_1}{24\beta}(\eta H)^4 + \eta H + \frac{1}{\beta}\left(\overline{P}_{\eta H} - \overline{P}_H\right) \qquad \text{(A11)}$$

$$\xi_3 = \frac{(b_1-b_2)}{2}(\eta H)^2 + \frac{b_2}{2}H^2 + (1-\eta)a_2H \qquad \text{(A12)}$$

$$\overline{P}_{\eta H} = \frac{b_2}{24}(\eta H)^4 + \frac{a_2}{6}(\eta H)^3 + \frac{R_{\eta H}}{2}(\eta H)^2 - P_H(\eta H) \qquad \text{(A13)}$$

$$\overline{P}_H = \frac{b_2}{24}H^4 + \frac{a_2}{6}H^3 + \frac{R_{\eta H}}{2}H^2 - P_H H \qquad \text{(A14)}$$

$$P_H = \frac{b_2}{6}H^3 + \frac{a_2}{2}H^2 + R_{\eta H}H \qquad \text{(A15)}$$

$$R_{\eta H} = \frac{(b_1-b_2)}{2}(\eta H)^2 - a_2(\eta H) \qquad \text{(A16)}$$

Appendix C: Derivation of Model 3

Equation (7a) has also been derived analogously, in which the compatibility condition of displacements at $z = \eta H$ is observed in addition to the boundary conditions. This involves a much more lengthy mathematical work. Only at one stage in the process of derivation of the model, a term involving the product of the quantity $e^{-\zeta H}$ and another negligibly small quantity is assumed zero. Considering the relatively large value of ζ used for the best-fitting curve and the rather small value of the coefficient of $e^{-\zeta H}$, this approximation is easily justified. Only the final forms of the coefficients are given below for the sake of brevity:

$$\lambda = \frac{b_1}{2}\left[\frac{(\eta H)^3}{3} + \frac{vr}{\zeta} e^{-\zeta\eta H}\left(\eta^2 H^2 + \frac{2}{\zeta}\eta H + \frac{2}{\zeta^2}\right)\right] - \frac{vrb_1}{\zeta^3}$$
$$- vr\left[\frac{a_2}{\zeta}\left(\eta H + \frac{1}{\zeta}\right) + \frac{b_2}{2\zeta}\left(\eta^2 H^2 + \frac{2}{\zeta}\eta H + 2\zeta^2\right) + \frac{R_{\eta H}}{\zeta}\right] e^{-\eta\zeta H} + P_H - P_{\eta H} \quad \text{(A17)}$$

$$\delta = H - \frac{vr}{\zeta} \quad \text{(A18)}$$

$$R_{\eta H} = \frac{(b_1 - b_2)}{2}(\eta H)^2 - a_2(\eta H) \quad \text{(A19)}$$

$$P_H = \frac{a_2}{2} H^2 + \frac{b_2}{6} H^3 + R_{\eta H} H \quad \text{(A20)}$$

$$P_{\eta H} = \frac{a_2}{2}(\eta H)^2 + \frac{b_2}{6}(\eta H)^3 + R_{\eta H}\eta H \quad \text{(A21)}$$

$$\kappa_1 = \frac{\delta}{\lambda}\left\{-\tilde{P}_{\eta H} - \frac{vr}{\zeta^2} e^{-\zeta\eta H}\left[a_2\left(\eta H + \frac{2}{\zeta}\right) + R_{\eta H} + \frac{b_2}{2} T_{\eta H}\right]\right\}$$
$$+ \left(\frac{\delta}{\lambda} P_H + H\right)\eta H + \frac{\delta}{\lambda}\tilde{P}_H - \frac{H^2}{2} - \frac{\delta}{\lambda} P_H H$$
$$+ \frac{b_1\delta}{2\lambda}\left(\frac{\eta^4 H^4}{12} - \frac{vr}{\zeta^2} T_{\eta H} e^{-\zeta\eta H}\right) - \left(\frac{vrb_1\delta}{\lambda\zeta^3} + \frac{vr}{\zeta}\right)\eta H + \frac{3b_1}{\lambda}\frac{vr\delta}{\zeta^4} + \frac{vr}{\zeta^2} \quad \text{(A22)}$$

$$\kappa_2 = \frac{1}{\lambda}\left\{\tilde{P}_{\eta H} - \frac{vr}{\zeta^2} e^{-\zeta\eta H}\left[a_2\left(\eta H + \frac{2}{\zeta}\right) + R_{\eta H} + \frac{b_2}{2} T_{\eta H}\right] + P_H H(1-\eta) - \tilde{P}_H\right\}$$
$$- \frac{b_1}{2\lambda}\left(\frac{\eta^4 H^4}{12} - \frac{vr}{\zeta^2} T_{\eta H} e^{-\zeta\eta H}\right) + \left(\frac{vrb_1}{\lambda\zeta^3} + 1\right)\eta H - \frac{3b_1}{\lambda}\frac{vr}{\zeta^4} \quad \text{(A23)}$$

$$\kappa_3 = \frac{(b_1 - b_2)}{2}\eta^2 H^2 + a_2 H(1-\eta) + \frac{b_2}{2} H^2 \quad \text{(A24)}$$

$$T_{\eta H} = \eta^2 H^2 + \frac{4}{\zeta}\eta H + \frac{6}{\zeta^2} \quad \text{(A25)}$$

$$\tilde{P}_H = \frac{a_2}{6} H^3 + \frac{b_2}{24} H^4 + \frac{R_{\eta H}}{2} H^2 \quad \text{(A26)}$$

$$\tilde{P}_{\eta H} = \frac{a_2}{6}(\eta H)^3 + \frac{b_2}{24}(\eta H)^4 + \frac{R_{\eta H}}{2}(\eta H)^2 \quad \text{(A27)}$$

$$r = r_x + r_y \quad \text{(A28)}$$